A Wearable Electromagnetic Technology for the Detection and Diagnosis of Joint Effusion

Thesis

Presented in Partial Fulfillment of the Requirements for the Degree Bachelor of Science in Electrical and Computer Engineering with Honors Research Distinction of The Ohio State University

By

Zeke Z. Dalisky

Undergraduate Program in Electrical Engineering

The Ohio State University

2020

Thesis Committee:

Prof. Asimina Kiourti, Ph.D., Advisor

Prof. Paul Berger, Ph.D.

Abstract

Wearable electronics and advances in electromagnetics have the potential to revolutionize medical research and the healthcare industry by monitoring the body in a way that has minimal impact on the user. The current state-of-the-art medical imaging methods, including X-ray, ultrasound, and Magnetic Resonance Imaging (MRI), are each capable of providing high-resolution images of body internals but are very resource-intensive and primarily limited to specialized medical centers. A wearable method for detecting joint effusion, the buildup of synovial fluid within a joint, is introduced which addresses these shortcomings. This approach uses two conducting loops placed around the joint region to detect the size of effusion by monitoring changes in the transmission coefficient (S_{21}) from one loop to another, a product of the nearby dielectric properties. Through electromagnetic simulations on a simplified arm model containing a spherical effusion, the feasibility of this detection method is demonstrated. By analyzing simulation results, the design of the conducting loops is optimized to provide for the clearest trend between S_{21} and the effusion radius. It is shown that 0.5 cm variations in radius from 1 to 3 cm can be detected with S_{21} precision as low as 1.0234 dB for magnitude or 13.4985 degrees for phase. Future research is recommended to validate the concept experimentally and further improve upon the system.

Acknowledgments

The author would like to express his sincere thanks to Prof. Asimina Kiourti and the Wearable and Implantable Technologies (WIT) group for assisting with the conduction of this research. Special recognition is given to Vigyanshu Mishra for providing invaluable guidance throughout all stages of this project, and Katrina Guido for assisting with dielectric property measurement. The author would also like to thank Dr. Mathew Mathew of the University of Illinois at Chicago for providing a sample of bovine calf serum for use in this project.

Table of Contents

List of Tables

List of Figures

Chapter 1: Introduction

Over the past several decades, medical imaging has become an integral component of the healthcare industry and medical research [1]. Advancements in technologies such as X-ray, ultrasound, and magnetic resonance imaging (MRI) allow medical professionals to quickly view detailed images of the inside of the body for detecting or diagnosing medical conditions [1]. These systems, however, face shortcomings [2] including the large size of equipment, high production and usage expense, availability limited to medical centers, and oftentimes exposure to ionizing radiation. A diagnostic imaging tool which addresses each of these concerns would be more accessible than these popular technologies and could introduce the benefit of long-term monitoring away from hospitals. Wearable electronics show great promise for many medical applications due to their low cost, inherent portability, and minimal impact on the user [3]. These advantages allow for new solutions to be developed which address the ever-present need for medical detection and diagnosis.

Joint effusion, pictured in Fig. 1, is a medical condition that occurs with abnormal fluid buildup in or around a joint, with varying causes including trauma, arthritis, or infection [4]. Detection and diagnosis of joint effusion is typically performed via a combination of physical examination, medical imaging (X-ray, ultrasound, or MRI), and extraction of the synovial fluid (which is present in joints) from the affected joint for

laboratory analysis (arthrocentesis) [4]. This process requires appropriate medical facilities and staff, is intrusive to the affected region, and does not allow for changes in the effusion to be monitored over time.

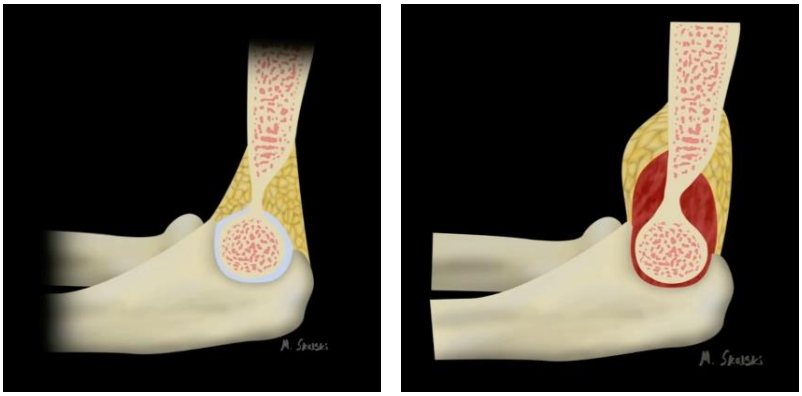

Figure 1: Depiction of Joint Effusion in the Elbow [5].

Previous work [6] in detecting edema in the brain, a complication that is also related to fluid buildup, has employed inductive phase shift spectroscopy as an alternative to traditional imaging methods. However, this approach is limited only to low frequencies and detection of small (<6 degrees) changes in phase, something the proposed method intends to improve upon.

This research introduces a wearable technology for detecting and diagnosing joint effusion by wirelessly monitoring the electromagnetic behavior of the joint region using the magnitude and phase of transmission between two conducting loops. The primary goal of this project was to determine how volume of synovial fluid in a joint, as well as any changes, can be detected wirelessly using a wearable device. Additionally, this project serves as a trial run for this type of technology, which can be adapted for other medical conditions or developed further into a more general wearable imaging system.

The remainder of this thesis is organized as follows:

- Chapter 2 describes the concept of the technology and outlines its operating principles.
- Chapter 3 introduces the model used for addressing joint effusion.
- Chapter 4 describes the design process used to apply the technology introduced to monitoring joint effusion.
- Chapter 5 discusses the results of key CST simulations for detecting joint effusion using this technology.
- Chapter 6 highlights conclusions made from this research.
- Chapter 7 provides suggestions and ideas for further work.

Chapter 2: Operating Principle

The proposed method for detecting joint effusion relies on monitoring the dielectric behavior of the joint region. Within this medium, the underlying biological materials (e.g. synovial fluid, muscle, bone), each with its own frequency-dependent permittivity and conductivity values, affect the propagation of electromagnetic waves. Evidently, changes in the amount or type of each material within the joint region will correspond to changes in how waves are able to propagate through it. To monitor these changes, two loops of wire are positioned around a joint as shown in Fig. 2 below, with one acting as a transmitter and the other acting as a receiver.

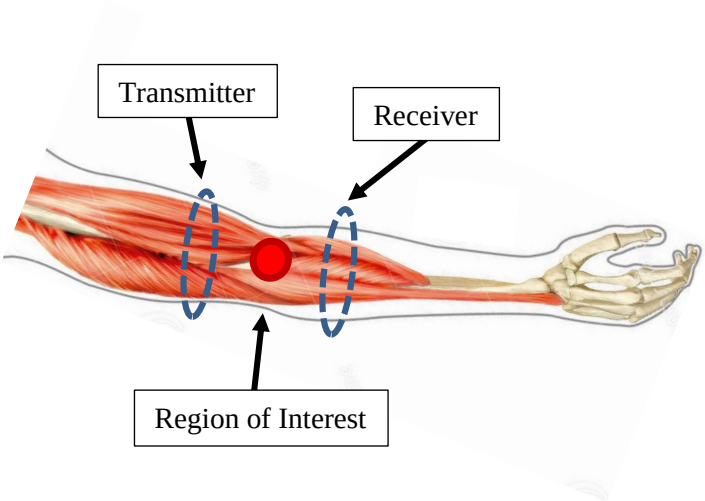

Figure 2: Example Placement of Loops Around Elbow.

The transmission coefficient S_{21} can be used to describe both the magnitude and phase of a signal sent from the transmitting loop to the receiving loop over a spectrum of frequencies. A key goal of this research is to determine how the transmission coefficient (magnitude and/or phase) relates to the accumulation of synovial fluid and determine how to best use this measurement to identify the fluid volume.

Chapter 3: Modeling Joint Effusion

3.1. Simplified Joint Effusion Model in CST

In order to develop and simulate the proposed technology, an elbow effusion model was created using basic geometric shapes as shown in Fig. 3 consisting of muscle tissue, bone, and synovial fluid. Estimating the size of a typical human arm near the elbow, the arm muscle and bone were represented by concentric cylinders with 3.9 cm and 1 cm radii, respectively, and a length of 30 cm. At the center of the arm, a spherical ring of synovial fluid with a variable radius surrounds the bone. The radius of the sphere can be increased to simulate the buildup of synovial fluid characteristic to joint effusion.

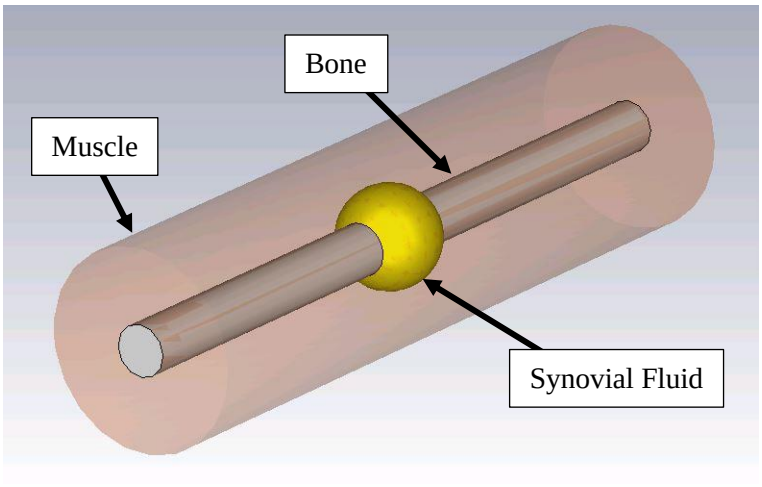

Figure 3: Joint Effusion Arm Model in CST

In practice, inherent differences in the dimensions or shape of different joints would have an effect on the design and simulation results of the proposed technology, however this model was used for all future simulations as an initial demonstrative case.

3.2. Selection of Material Properties

Dielectric properties up to 2 GHz were included for each material in the CST simulation model. Muscle and bone properties were each downloaded from the IFAC's database for the Dielectric Properties of Body Tissues [7]. A combination of 20% cancellous bone and 80% cortical bone was used throughout the bone cylinder as an approximation of the typical makeup of the joint region [8]. Since the dielectric properties of synovial fluid vs. frequency have not yet been reported, additional measurements were necessary.

Bovine Calf Serum (BCS) has been used in numerous studies [9,10,11] as a substitute for synovial fluid due to its increased accessibility. Similarities in both physical properties such as viscosity [9] and the material composition [10] of each substance suggest that BCS could serve as a reasonable dielectric approximation for synovial fluid. The relative permittivity and loss tangent of a BCS sample, provided by Dr. Mathew of the University of Illinois at Chicago, were measured using a probe and network analyzer as pictured in Fig. 4. The sample contained a 30 g/L protein concentration, the mean value for synovial fluid shown in literature to best resemble genuine synovial fluid mechanically [11].

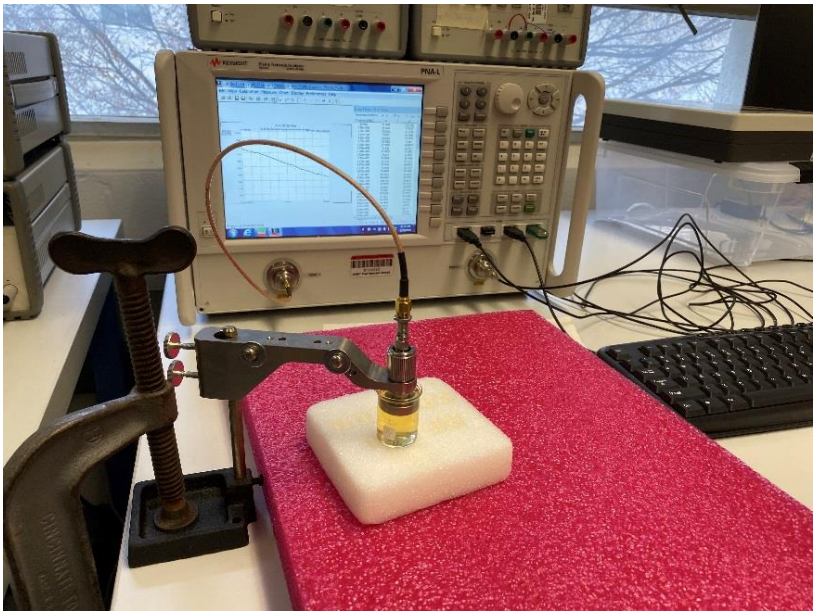

Figure 4: Experimental Setup for Measuring the Dielectric Properties of BCS

Dielectric properties of the BCS were measured from 200 MHz to 3 GHz. Seven trials were averaged together to reduce error. The relative permittivity of the BCS fell between water and blood, two similar biological liquids with known properties [7], at these frequencies while the loss tangent of BCS was slightly greater. A comparison of the dielectric properties for each of the model's components is shown in Fig. 5.

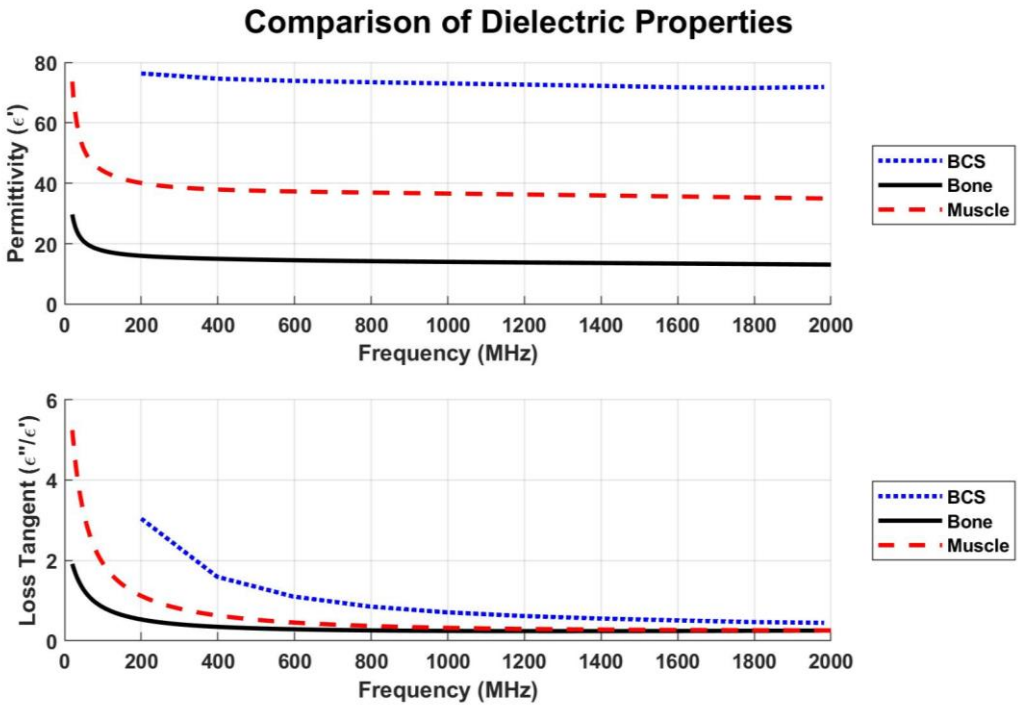

Figure 5: Dielectric Properties of Arm Model Materials

Chapter 4: Design Methodology

4.1. Simulation Method and Performance Metrics

The process for determining how to best monitor joint effusion using this technology primarily consisted of performing simulations in the Computer Simulation Technology (CST) Microwave Studio. Once the model for a given design was created and fitted with a tetrahedral mesh, as seen in Fig. 6, the frequency-domain solver was used to calculate the transmission coefficient between from 200 MHz to 2 GHz while a parametric sweep was performed on the BCS sphere's radius from 1 cm to 3 cm in 0.5 cm increments. Due to the presence of the 1 cm radius bone cylinder through the BCS sphere, the 1 cm radius case contains actually contains no fluid while increasing the radii causes BCS buildup. In general, after simulations were performed over a wide range of frequencies, they were repeated at a reduced frequency range of interest to provide higher accuracy.

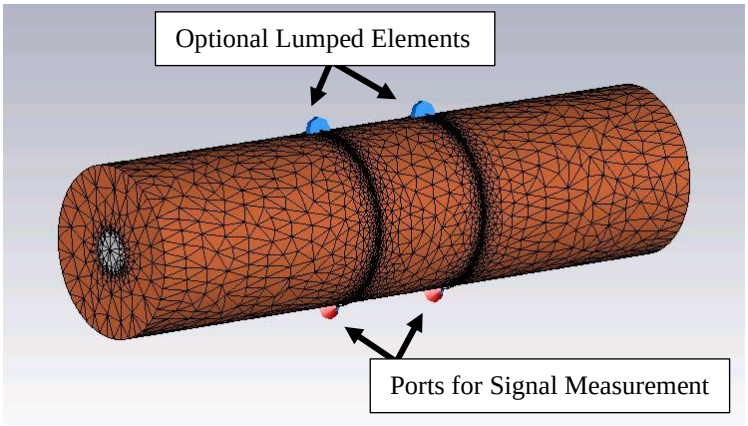

Figure 6: Simulation Setup in CST

In order to meaningfully correlate the transmission coefficient S_{21} to the volume of synovial fluid, the results of a given design simulation should include a clear trend between BCS radius and the magnitude or phase of S_{21} at a given frequency. That is, S_{21} should increase with increasing radii or decrease with increasing radii for all radii in the simulation. Once this trend is established, the performance of a design at a given frequency can be evaluated based on how much S_{21} changes with radius. A greater dependence, discernable by a greater separation between lines of a simulation's results, indicates that the technology is more sensitive. This means that a given change in BCS volume could be detected using less precise S_{21} measurements, or that a smaller change in BCS volume could be detected using a given precision in S_{21} measurement.

While evaluating the results of many different simulations during design, it became apparent that the total trend range, i.e. the change in magnitude or phase of S_{21} between the smallest and largest radii at a given frequency, was a poor indicator of how well a specific frequency or design could be used to monitor the amount of BCS. This is because the relationship between radius and S_{21} was often sporadic, meaning, for example, that while it may be easy to observe a change in S_{21} when the radius increases from 2 cm to 2.5 cm, there may be almost no change in S_{21} from 2.5 cm to 3 cm. To account for this behavior, the change in S_{21} at each radius interval had to be considered. Using the MATLAB code in Appendix A, frequency ranges which contain a trend in S_{21} magnitude or phase vs. radius were first determined for the results of a specific simulation. Within each of these ranges, the change in S_{21} between each radius interval (i.e. 1 to 1.5 cm, 1.5 to 2 cm, etc.) was calculated vs. frequency. The frequencies with the

greatest minimum S_{21} differentials were identified for each magnitude or phase trend range. These are the optimal operating frequencies where the system is most sensitive. By comparing the relationship between radius and S_{21} at this operating frequency for different simulations, designs can be evaluated.

Other factors were also considered while evaluating the simulation results of a specific design. Although relative changes in S_{21} are of most interest, the absolute magnitude of S_{21} is also relevant because detecting changes in weaker signals could be more difficult to implement when using hardware to implement this technology. Additionally, some attention was given to the bandwidth of each S_{21}-radius trend, the range of frequencies where S_{21} is strictly increasing or decreasing with radius. Even though ideally the trend only needs to exist at a single frequency for fluid detection, if the frequency range is especially small (e.g. a few MHz vs. a few hundred MHz), any simulation or measurement errors that would effectively shift the S_{21} frequency spectrum of the system or model could potentially eliminate the trend. While systematically identifying trends in MATLAB, only regions wider than approximately 20 MHz were considered.

4.2. Loop Design Variables

All loops considered were made from 30 AWG (0.254 mm-diameter) copper wire. The main variables that were considered while determining how to best detect and monitor joint effusion were loop placement and the potential addition of a capacitor or inductor. Two options were considered for how the loops would be positioned: wrapped around the arm on either side of the joint or longitudinal to the arm cylinder on either side

of the joint as depicted in Fig. 7. Preliminary simulations showed that the longitudinal placement provided similar radius-S_{21} trends, however this setup would be less practical for a wearable than having the wrap-around loop as it would be more difficult to securely mount the loop overlapping the joint without interfering with movement, so the first option was chosen. The loop radius was fixed at 4 cm to fit the 3.9 cm arm radius.

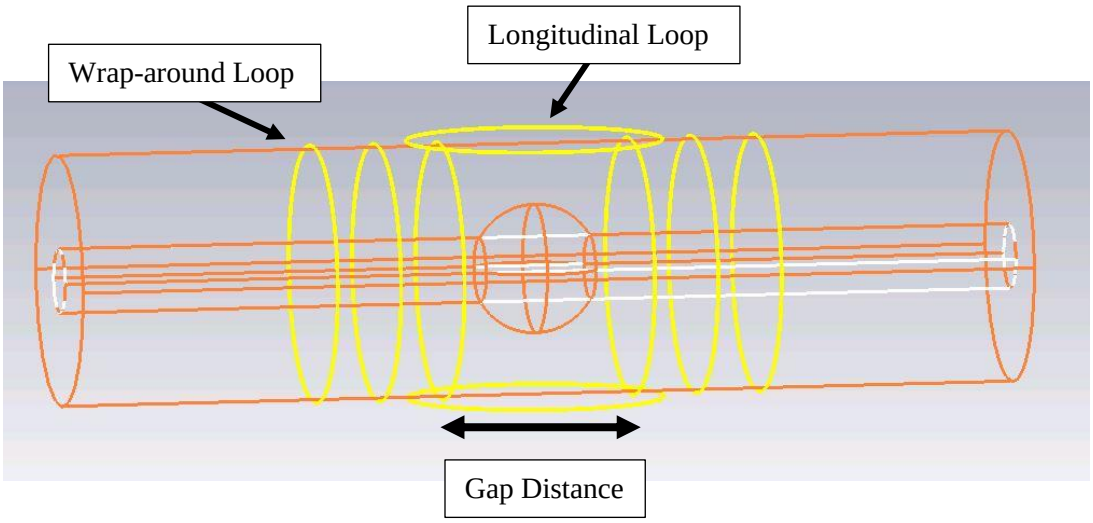

Figure 7: Loop Placement Options

The distance between loops remained a variable to be optimized in simulation. For any gap distance, it was assumed that the joint fluid was centered between the loops, as changing the sphere location affects the trend at a design's operating frequency. Additionally, since sphere sizes up to 6 cm in diameter were being considered, the gap was set at a minimum of 6 cm to ensure that the sphere is always contained between the loops. Gaps smaller than this were still able to pick up on changes in volume during simulation and exhibited a higher S_{21} magnitude due to the loops being closer together, however the trends at higher radii were less pronounced and the placement of these loops

in a wearable would overlap the elbow itself, likely causing issues with mobility. Future improvements may be possible to detect and measure fluid with an unknown offset from the center as mentioned in Chapter 7.

The addition of a capacitor or inductor to the loop was also considered. This element would be added in series, and the reactance of this element would allow for the conducting loop to become resonant at a specific frequency. To tune the resonance frequency of the loop, an element was selected according to $\omega = \frac{1}{\sqrt{LC}}$ such that its reactance cancels the reactance of the loop, shown in Fig. 8, at the desired frequency. Notably, frequencies for which the loop is inductive, up to approximately 400 MHz, require a capacitor for tuning while frequencies from approximately 400-1000 MHz require an inductor. To allow for future experimental validation, only widely available through-hole component values were considered for these elements, based on availability from Digi-Key [12].

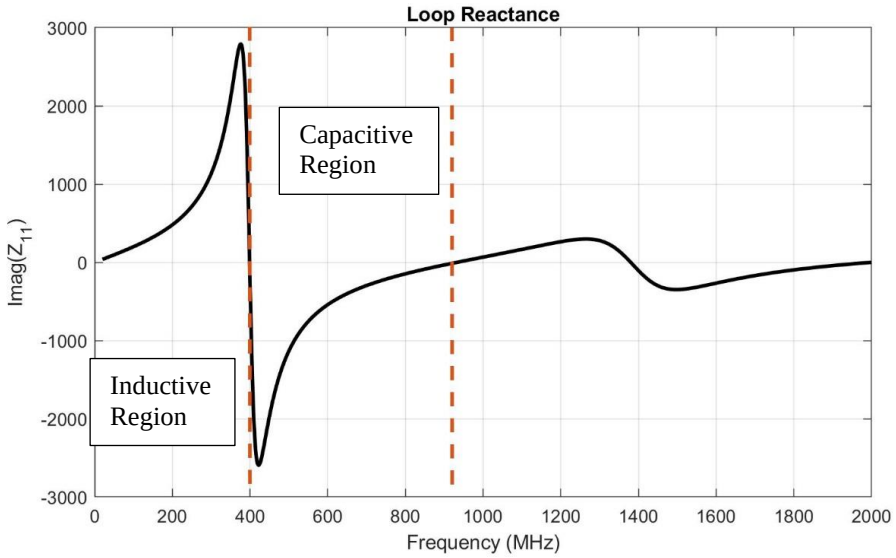

Figure 8: Reactance of a Single Loop

Chapter 5: Simulation Results and Discussion

As outlined in Chapter 4, simulations were performed to optimize the trend between radius and the transmission coefficient of the two loops. First, the distance between coils was varied. Gaps of up to 12 cm demonstrated trends in S_{21} magnitude or phase vs. radius, but it was clear that the relative changes in S_{21} were greatest with a 6 cm gap, which also inherently had the highest transmission magnitude.

Fig. 9 shows the simulation results from using basic loops (without the addition of a reactive component) with a 6 cm gap over the full 200-2000 MHz spectrum. Multiple different trend regions are present for both the magnitude and phase plots. The best trend in S21 magnitude occurs at the lower end of the spectrum at 568.46 MHz, requiring a precision of 0.45 dB to detect the 0.5 cm changes in radius, while the best phase trend occurs at 1514.90 MHz and requires a precision of 8.60 degrees.

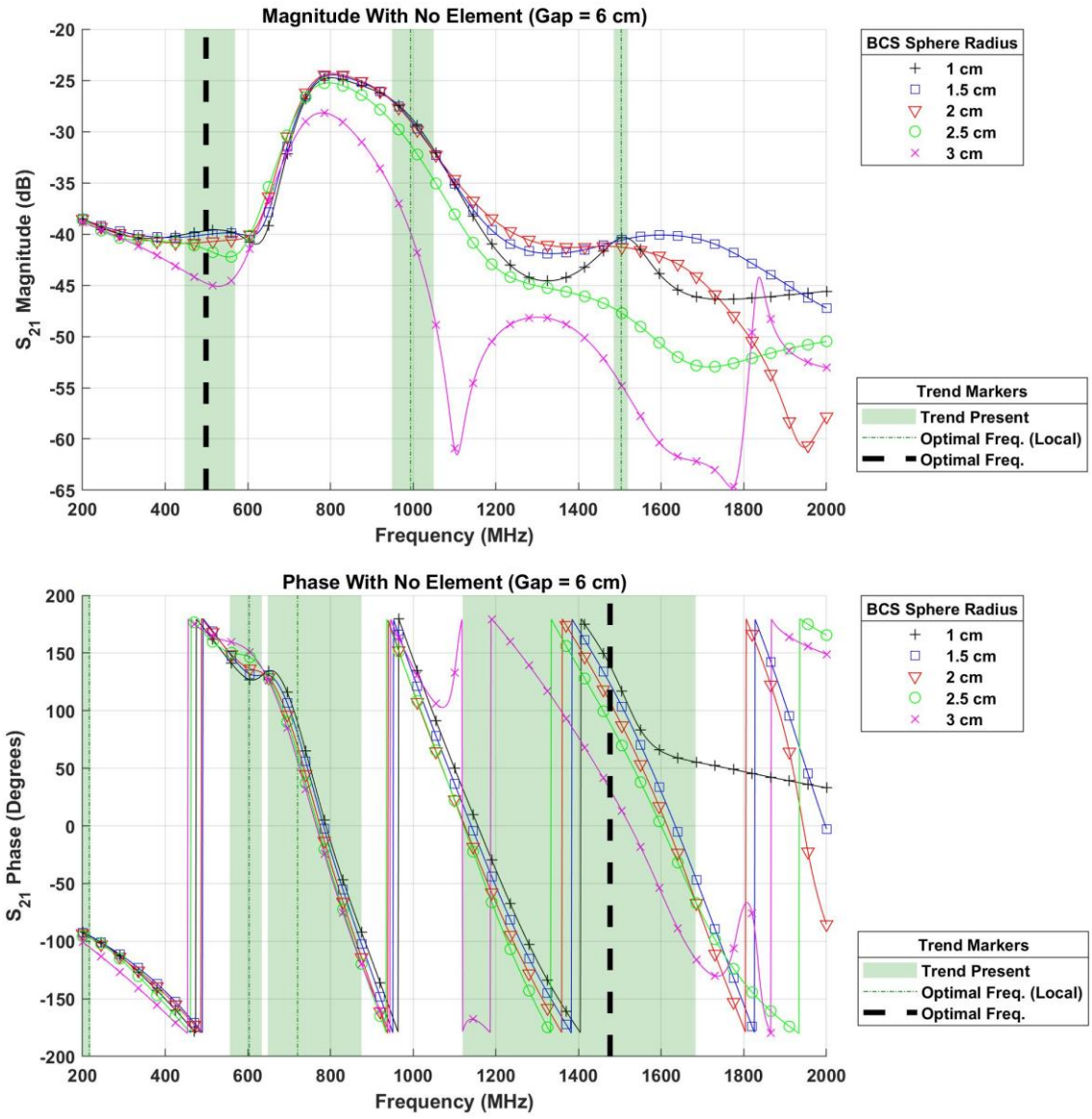

Figure 9: Simulation Results without Element and 6 cm Gap

Next, a capacitor was added to the loop to determine if making the loop resonant can improve its radius detection capabilities. In preliminary simulations, trends showed visual improvement as capacitance was lowered, pushing the resonance frequency

towards the peak in the loop reactance seen in Fig. 8. The results in Fig. 10 use the lowest valued capacitor available, a criterion mentioned in Section 4.2, of 1 pF corresponding to a resonance frequency of approximately 240 MHz. At this frequency, the magnitude of S_{21} is maximized and there is very little distinction between the phase of each radius.

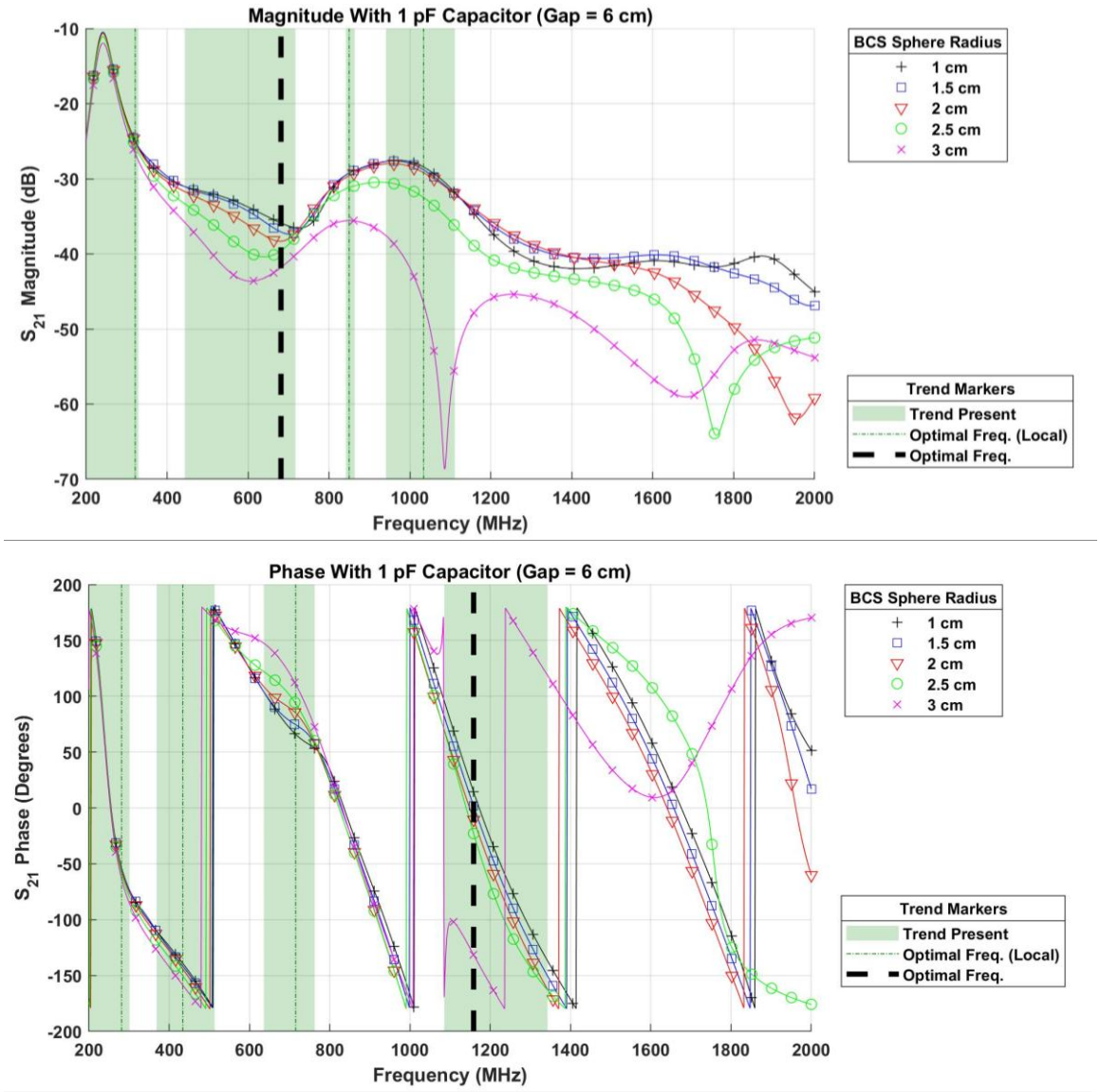

Figure 10: Simulation Results with 1 pF Capacitor and 6 cm Gap

Above resonance, the overall shape of the plot is similar to without a capacitor, but there is some variance which makes it possible for one of the designs to perform better than the other. The best magnitude trend occurred at 681.32 MHz, requiring a sensitivity of 1.18 dB, while the best phase trend occurred at 1158.50 MHz, requiring a sensitivity of 12.19 degrees.

The capacitor was finally replaced with an inductor. Again, trends appeared to improve as inductance was increased, moving resonance frequency towards the region of peak negative reactance. An inductance of 820 nH corresponds to resonance closest to the loop reactance minimum, at approximately 415 MHz. As seen in Fig. 11, there is once again a peak in magnitude and narrow range of phases at resonance. Only one region has a significant trend in magnitude, with an optimal frequency of 568.46 MHz requiring 0.49 dB sensitivity. The best phase trend is at 1514.90 MHz and requires a phase sensitivity of 8.59 degrees.

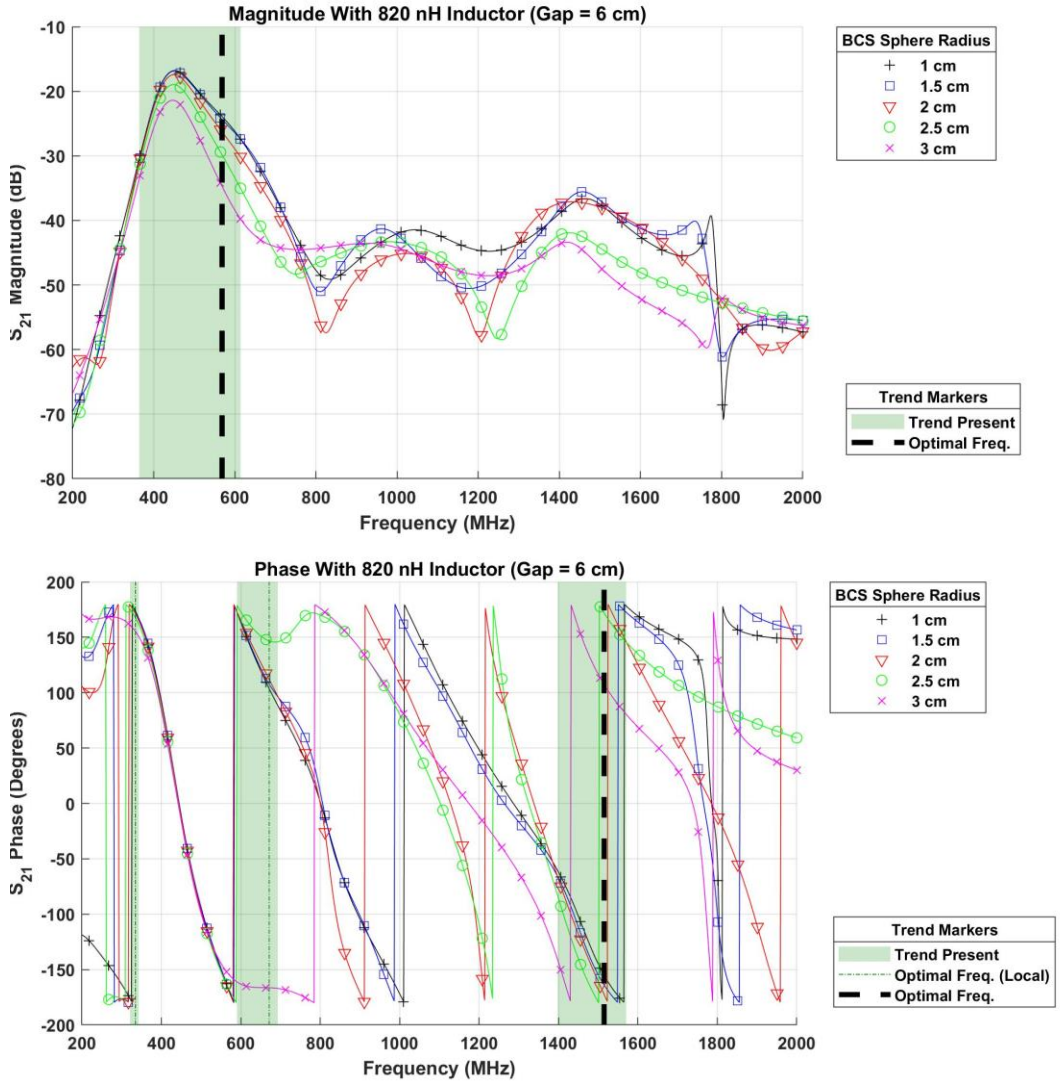

Figure 11: Simulation Results with 820 nH Inductor and 6 cm Gap

In order to compare the best S_{21} vs. radius trends identified in each of the three designs with a higher degree of accuracy, simulations were performed again within a <300 MHz range near each optimal frequency. Component tolerance was also considered. A comparison of the magnitude and phase trends for the cases without an

additional element, with a 1 pF (± 0.25 pF) capacitor, and with an 820 nH (±10%) inductor can be seen in Fig. 12.

For each of these setups, the optimal frequency and required sensitivity changed slightly from the simulations over a broader frequency range. A summary of this data can be seen in Table 1. Variance in the lumped element values due to tolerance notably had a much greater impact on S_{21} magnitude than phase. As expected, the magnitude trends improved when capacitance decreased and when inductance increased. The magnitude variations due to capacitor tolerance are much more pronounced likely due to the greater percent change in the capacitance (±25% vs. ±10%) and the available inductor value being closer to an optimal value than the available capacitor by resonating at a frequency closer to the target peak in reactance seen in Fig. 8.

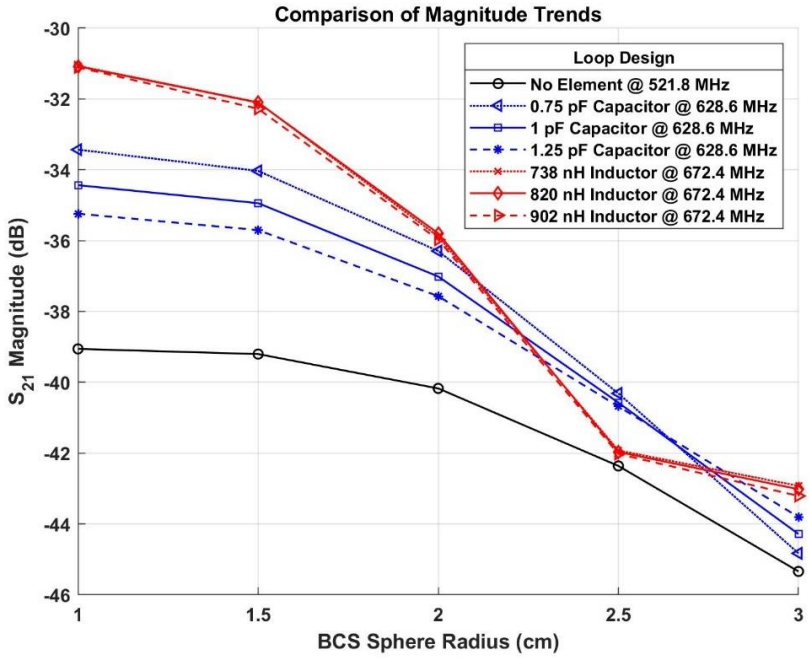

(a)

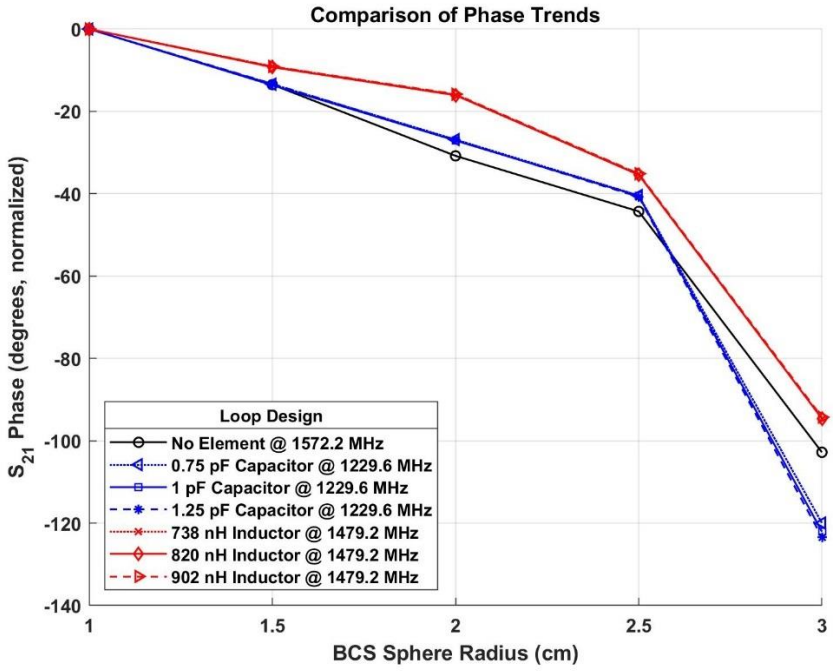

(b)

Figure 12: Comparison of S21 (a) Magnitude and (b) Phase vs. Radius Trends

Table 1: Summary of Best Trend for Each Design with Improved Accuracy

Component Added	Magnitude Trend		Phase Trend	
	Freq. (MHz)	Req. Sens. (dB)	Freq. (MHz)	Req. Sens. (deg)
None	521.8	0.1460	1572.2	13.4985
1 pF Capacitor	628.6	0.5081	1229.6	13.4549
(+ 0.25 pF)	|	0.4634	|	13.3137
(- 0.25 pF)	|	0.5994	|	13.4028
820 nH Inductor	672.4	1.0234	1479.2	6.8046
(+ 82 nH)	|	1.1699	|	6.7458
(- 82 nH)	|	1.0001	|	6.8410

Based on the sensitivity requirements of each design, the best method for detecting sphere radius using the magnitude of S_{21} is to use an 820 nH inductor and an operating frequency of 672.4 MHz, requiring a measurement precision of at least 1.0234 dB to differentiate each 0.5 cm radius interval. For detecting sphere radius using phase, however, it is best to use a loop with no added elements and an operating frequency of 1572.2 MHz, requiring a precision of at least 13.4985 degrees. Although the selected magnitude trend has very low variation due to inductor tolerance, the phase trend inherently has none and would ultimately be much easier to construct due to simply being a wire loop.

Chapter 6: Conclusion

A new method for detecting and monitoring the size of joint effusion is introduced. Using two conducting loops placed on either side of a joint, changes in the amount of synovial fluid, which affect the dielectric properties of the joint region, are detected in the transmission coefficient (S_{21}) between the loops. Compared to the imaging methods typically used to monitor effusion (i.e. X-ray, ultrasound, or MRI), which are very resource intensive and require specialized testing facilities, this technology is intended to be used in a wearable device which can provide unobtrusive, continuous monitoring.

A simplified arm model was constructed in CST to evaluate the feasibility of this method in simulation and allow for an investigation into how the loops should be designed and placed. By comparing the trends in S_{21} vs. effusion radius at a given frequency for different possible designs, design decisions could be made. The minimum required precision in magnitude (dB) or phase (degrees) to detect each effusion radius served as a key performance metric. It was determined that the loops should be wrapped around the arm, as close to the effusion region as possible without overlapping it. Additionally, it was discovered that adding a reactive element to the loop to make it resonant improved the system's ability to differentiate effusion radii using the magnitude of S_{21}. Ultimately, this detection method is very promising and warrants future research.

Chapter 7: Future Work

This research focused primarily on applying the core detection concept to a joint effusion model in simulation, however future work could be done to provide experimental validation, improve the detection capabilities, and further develop the technology into a complete wearable device.

7.1. Proposed Method for Experimental Validation

Experimental validation of the detection method introduced can be conducted using a similar setup to the simulations, with a tissue-emulating phantom as the arm model and a network analyzer to measure and record the transmission coefficient between loops. To simplify the construction of the phantom in this experiment, it is recommended that the bone cylinder be removed. This simplification inherently affects the simulation results, however as shown in Fig. 13, for example, the same process can be used to find the best trend in S_{21} and radius. In this case an additional sphere radius of 0.5 cm is also considered; however, the analysis process remains the same for any combination of radii. For this model, the best magnitude trend ends up occurring without a capacitor or inductor near 1492.4 MHz and requires a 0.6870 dB sensitivity for radius detection.

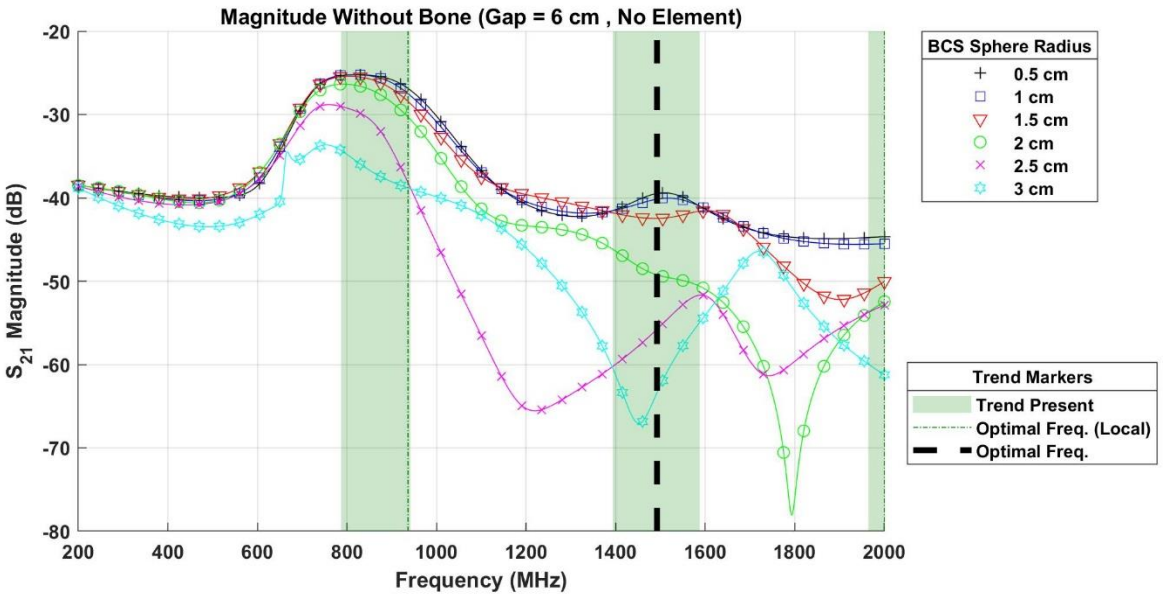

Figure 13: Sample Result from Simulation without Bone

To construct the simplified arm, raw ground beef can be enclosed within a 3D-printed cylinder with inner dimensions to match the simulation model. A potential 3D structure is shown in Fig. 14 which comes apart at the middle to allow for easier printing and setup and includes small indents at 0.5 cm intervals to assist with loop placement.

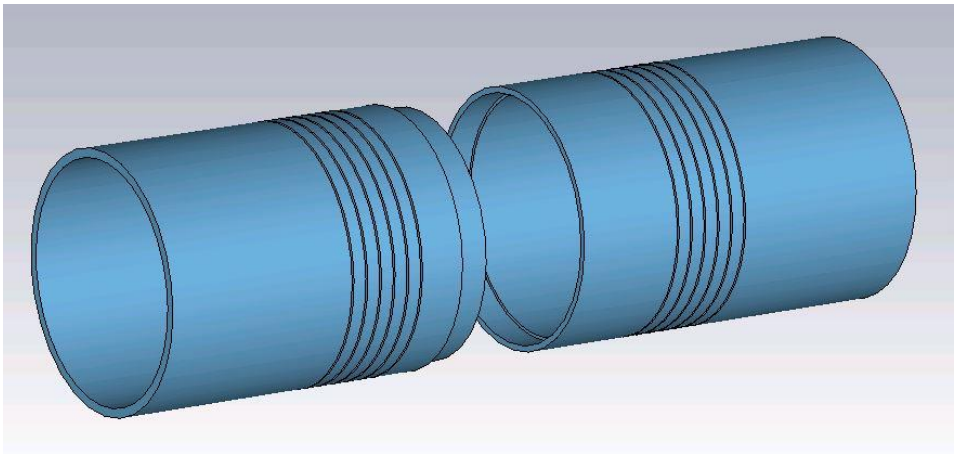

Figure 14: 3D Arm Structure for Phantom Construction

The effusion itself can be realized experimentally by filling a balloon with target volumes of liquid and placing it at the center of the arm cylinder, molding the beef to ensure a spherical shape. Use of 3D printed sphere shell was also considered, however initial simulations showed that the resin shell itself would cause significant variations in S_{21} for different radii. Due to the safety and storage concerns regarding biological materials such as BCS, a mixture of water, salt, and sugar was developed which closely replicates its permittivity and loss tangent in the frequency range of interest. Noting that adding sugar primarily decreases the relative permittivity while adding salt primarily increases the conductivity [13], each was added to water in small increments as the measured dielectric properties of each new mixture approached the values measured for BCS. As shown in Fig. 15, a mixture of 0.35 M salt and 0.35 M sugar is able to closely match the properties of BCS.

After determining and constructing the final experimental setup, the dielectric properties of each material can be measured and uploaded into the simulation model to ensure a close match between materials in simulation and the experiment.

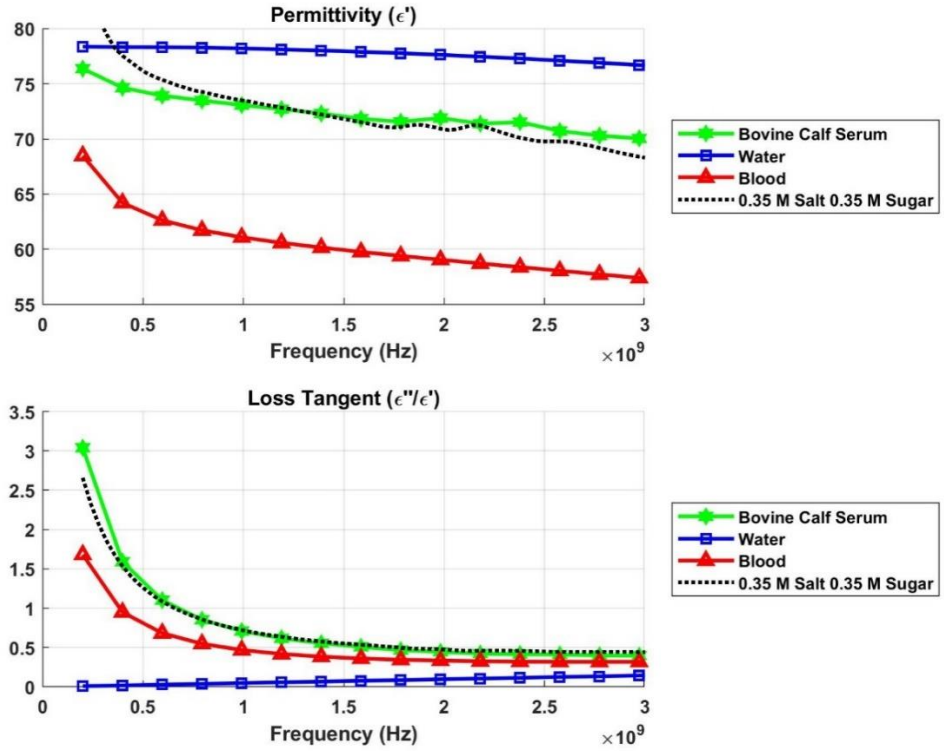

Figure 15: Dielectric Properties of a Sugar-Salt Mixture for Replicating Bovine Calf Serum

7.2. Potential Features and Improvements

Several different directions can be taken to further improve upon the joint effusion detection method presented. One improvement could involve being able to detect changes the material composition of the synovial fluid, in addition to its volume. This would be useful because joint diseases which typically cause joint effusion to occur may also have an effect on the biological makeup of the synovial fluid, requiring it to be extracted for lab analysis [14]. Additionally, detecting position could be useful in cases when the exact location of effusion is unknown from the outside. A possible approach to

this problem could involve using more than two loops and comparing the transmission coefficient between different loop pairings. More than two loops could also be used to provide measurements from multiple gap distances at the same time, potentially allowing for improved accuracy.

References

[1] M. Nadeski and G. Frantz, "Future of Medical Imaging," in *Medical Imaging*, K. Iniewski and T. Farncombe, Eds. Boca Raton, FL: CRC Press, 2014. [E-book] Available: Safari Books Online.

[2] L. Baker, "Medical Imaging Capacity and Health Care Spending," *Essays on Trends, Innovative Ideas and Cutting-Edge Research in Health Care*, Nov. 2007. [Online]. Available: NIHCM Foundation, www.nihcm.org.

[3] M. Stoppa and A. Chiolerio, "Wearable Electronics and Smart Textiles: A Critical Review," *Sensors*, vol. 14, pp. 11957-11992, 2014. [Online]. Available: www.mdpi.com/journal/sensors.

[4] M. Johnson, "Acute Knee Effusions: A Systematic Approach to Diagnosis," *American Family Physician*, vol. 61/8, pp. 2391-2400, April 2000. [Online]. Available: www.aafp.org/journals/afp.

[5] H. Knipe and A. Dixon, "Elbow Joint Effusion", 2013. [Online]. Available: www.radiopaedia.org/articles/elbow-joint-effusion

[6] C. González and B. Rubinsky, "The detection of brain oedema with frequency-dependent phase shift electromagnetic induction," *Physiological Measurement*, vol. 27, pp. 539-552, 2006. [Online]. Available: https://www.ncbi.nlm.nih.gov/pubmed/16603802

[7] D. Andreuccetti, R. Fossi and C. Petrucci, "An Internet resource for the calculation of the dielectric properties of body tissues in the frequency range 10

Hz - 100 GHz". IFAC-CNR, Florence (Italy), 1997. Based on data published by C. Gabriel et al. in 1996. [Online]. Available: http://niremf.ifac.cnr.it/tissprop/

[8] "Structure and composition of bone," University of Cambridge DoITPoMS, Cambridge, UK, 2020. [Online]. Available: https://www.doitpoms.ac.uk/tlplib/bones/structure.php

[9] C. Myant and P. Cann, "On the matter of Synovial Fluid Lubrication: Implications for Metal-on-Metal Hip Tribology," Journal of the Mechanical Behavior of Biomedical Materials, vol. 34, pp. 338-348, June 2014. [Online]. Available: https://www.sciencedirect.com/

[10] J.M. Brandt, L.K. Briere, J. Marr, S.J. MacDonald, R.B. Bourne, and J.B. Medley, "Biochemical comparisons of osteoarthritic human synovial fluid with calf sera used in knee simulator wear testing," Journal of Biomedical Materials Research Part A, vol. 94/3, pp. 961-971, July 2010. [Online]. Available: https://onlinelibrary.wiley.com/

[11] E. Bortel, B. Charbonnier, and R. Heuberger, "Development of a Synthetic Synovial Fluid for Tribological Testing," Lubricants, vol. 3, pp. 664-686, Dec 2015. [Online]. Available: www.mdpi.com/journal/lubricants

[12] "Electronic Component Products," Digi-Key, Thief River Falls, MN. [Online]. Available: https://www.digikey.com/products/en

[13] K. Ito, K. Furuya, Y. Okano, and L. Hamada, "Development and Characteristics of a Biological Tissue-Equivalent Phantom for Microwaves," Electronics and

Communications in Japan, Part 1, vol. 84/4, pp.1126-1135, 2001. [Online]. Available: https://onlinelibrary.wiley.com/

[14] A. Dyszkiewicz, P. Janik, and M. Janik, “Preliminary Dielectric Studies of Knee Swelling Fluid in the Case of Arthritis, Which is Hard to Diagnose,” Physiological Measurement, vol. 27, pp. 1345-1359, 2006. [Online]. Available: https://www.ncbi.nlm.nih.gov/pubmed/17135704

Appendix A: MATLAB Code for Trend Detection and Analysis

```
%% load results from file
clear;clc;
mag=load('results without element 6cm gap 1-3cm bcs radius mag.csv');%changed
for each set of simulation results
phase=load('results without element 6cm gap 1-3cm bcs radius
phase.csv');%creates a 1001x6 array (1 column freq, 5 columns s21)

%% plot magnitude results
mag_figure=figure;
title('Magnitude With No Element (Gap = 6 cm)'); %title changed with
hold on;
p1_mag=plot(mag(:,1),mag(:,2),'k');
p2_mag=plot(mag(:,1),mag(:,3),'b');
p3_mag=plot(mag(:,1),mag(:,4),'r');
p4_mag=plot(mag(:,1),mag(:,5),'g');
p5_mag=plot(mag(:,1),mag(:,6),'m');

%plot formatting
marker_distance=25;
m1=plot(mag(1:marker_distance:end,1),mag(1:marker_distance:end,2), 'k+');
m2=plot(mag(1:marker_distance:end,1),mag(1:marker_distance:end,3), 'bs');
m3=plot(mag(1:marker_distance:end,1),mag(1:marker_distance:end,4), 'rv');
m4=plot(mag(1:marker_distance:end,1),mag(1:marker_distance:end,5), 'go');
m5=plot(mag(1:marker_distance:end,1),mag(1:marker_distance:end,6), 'mx');
grid;
xlabel('Frequency (MHz)');
ylabel('S_{21} Magnitude (dB)');
set(gcf,'position',[680 360 860 420]);
set(gca,'FontWeight','bold');

%% evaluate magnitude results

%find frequency ranges with trend
trend_region_count_mag=0;
trend_length_mag=1;
clearvars trend_index_mag trend_region_lengths_mag trend_region_starts_mag;
required_sens_mag=0;
for i=1:1:length(mag(:,1))
    %evaulate each frequency to see if there is a trend

trend_down=(mag(i,2)>mag(i,3))&&(mag(i,3)>mag(i,4))&&(mag(i,4)>mag(i,5))&&(ma
g(i,5)>mag(i,6));

trend_up=(mag(i,6)>mag(i,5))&&(mag(i,5)>mag(i,4))&&(mag(i,4)>mag(i,3))&&(mag(
i,3)>mag(i,2));

    %if a trend is present, keep track of where it occurs and group it with
    %any adjacent trends to form a trend region
    if trend_down || trend_up
        if exist('trend_index_mag')==0
            trend_index_mag=i;
            trend_region_count_mag=1;
            trend_region_starts_mag=i;
        else
```

```
            trend_index_mag=[trend_index_mag i];
            if not(ismember((i-1),trend_index_mag))
                trend_region_count_mag=trend_region_count_mag+1;
                trend_region_starts_mag=[trend_region_starts_mag i];

                if exist('trend_region_lengths_mag')==0
                    trend_region_lengths_mag=trend_length_mag;
                else
                    trend_region_lengths_mag=[trend_region_lengths_mag
trend_length_mag];
                end
                trend_length_mag=1;
            else
                trend_length_mag=trend_length_mag+1;
            end
        end
    end
end

%if a trend was found, continue plotting and analyzing trends
if trend_region_count_mag>0
    trend_region_lengths_mag=[trend_region_lengths_mag trend_length_mag];

    %plot trend regions
    best_freqs=mag(trend_region_starts_mag,1);
    for j=1:1:trend_region_count_mag
        if trend_region_lengths_mag(j)>=10 %set to minimum desired trend
bandwidth
            xrange=[mag(trend_region_starts_mag(j),1)
mag(trend_region_starts_mag(j)+trend_region_lengths_mag(j)-1,1)];
            yrange=get(gca,'YLim');
            f1=fill([xrange(1) xrange(1) xrange(2) xrange(2)],[yrange
flip(yrange)],[0, 0.5, 0],'facealpha',0.2,'linestyle','none');

            %determine the change in s21 for each change in radius
            x_index_range=[trend_region_starts_mag(j)
trend_region_starts_mag(j)+trend_region_lengths_mag(j)-1];
            max_gap=zeros(1,4);
            max_index=zeros(1,4);
            gap=zeros(4,length(x_index_range));
            min_gaps=zeros(1,length(x_index_range));
            for
k=trend_region_starts_mag(j):1:(trend_region_starts_mag(j)+trend_region_lengt
hs_mag(j)-1)
                gap(1,k)=mag(k,2)-mag(k,3);
                gap(2,k)=mag(k,3)-mag(k,4);
                gap(3,k)=mag(k,4)-mag(k,5);
                gap(4,k)=mag(k,5)-mag(k,6);
                min_gaps(k)=min(abs(gap(:,k)));
            end

            %identify the frequency with the greatest minimum gap
            [best_min_gap,best_min_gap_index]=max(min_gaps);
            for m=1:1:4
```

```
                [max_gap(m),max_index(m)]=max(abs(gap(m,:)));
            end
            [min_max_gap,min_max_gap_index]=min(max_gap);
            best_freqs(j)=mag(best_min_gap_index,1);

            %update required sensitivity
            if best_min_gap>required_sens_mag
                required_sens_mag=best_min_gap;
                required_sens_freq_mag=best_freqs(j);
                required_sens_index_mag=best_min_gap_index;
                required_sens_region=j;
            end
        else
            %keep track of any trends that do not meet required bandwidth
            if exist('short_trends');
                short_trends=[short_trends j];
            else
                short_trends=j;
            end
        end
    end

    %remove best trend and any short trends from being plotted as a local
    %best
    if exist('short_trends')
        best_freqs([short_trends required_sens_region])=[];
    else
        best_freqs([required_sens_region])=[];
    end

    %plot location of the best trends for each region
    v1=plot([required_sens_freq_mag required_sens_freq_mag],yrange,'k--
','lineWidth',3);
    for j=1:1:length(best_freqs)
        v2=plot([best_freqs(j)
best_freqs(j)],yrange,'color',[0,0.5,0],'linestyle','-.');
    end

    clearvars short_trends trend_index_mag trend_length_mag
trend_region_lengths_mag trend_region_starts_mag x_index_range;
    clearvars best_freqs gap max_gap max_index min_max_gap min_max_gap_index
required_sens_region;
else
    disp('No Magnitude Trends Found');
end

%display key results
fprintf('Best Magnitude Trend Frequency: %f\n',required_sens_freq_mag);
fprintf('Required Magnitude Sensitivity: %f dB\n',required_sens_mag);

%add 2 plot legends
l1_mag=legend([m1 m2 m3 m4 m5],'1 cm','1.5 cm','2 cm','2.5 cm','3
cm','location','northeastoutside');
title(l1_mag,'BCS Sphere Radius');
```

```
if trend_region_count_mag>0
    ax=axes('Position',get(gca,'Position'),'Visible','Off');
    l2_mag=legend(ax,[f1 v2 v1],'Trend Present','Optimal Freq.
(Local)','Optimal Freq.','location','southeastoutside');
    title(l2_mag,'Trend Markers');
    set(gca,'FontWeight','bold');
end

clearvars xrange yrange trend_region_count_mag;
clearvars trend_down trend_up i j k m;
clearvars m1 m2 m3 m4 m5 p1_mag p2_mag p3_mag p4_mag p5_mag l1_mag
marker_distance l2_mag f1 v1 v2;

%% plot phase results
phase_figure=figure;
title('Phase With No Element (Gap = 6 cm)');%title changed with simulation
results
hold on;
p1=plot(phase(:,1),phase(:,2),'k');
p2=plot(phase(:,1),phase(:,3),'b');
p3=plot(phase(:,1),phase(:,4),'r');
p4=plot(phase(:,1),phase(:,5),'g');
p5=plot(phase(:,1),phase(:,6),'m');

%format plot
marker_distance=25;
p1=plot(phase(1:marker_distance:end,1),phase(1:marker_distance:end,2), 'k+');
p2=plot(phase(1:marker_distance:end,1),phase(1:marker_distance:end,3), 'bs');
p3=plot(phase(1:marker_distance:end,1),phase(1:marker_distance:end,4), 'rv');
p4=plot(phase(1:marker_distance:end,1),phase(1:marker_distance:end,5), 'go');
p5=plot(phase(1:marker_distance:end,1),phase(1:marker_distance:end,6), 'mx');
grid;
xlabel('Frequency (MHz)');
ylabel('S_{21} Phase (Degrees)');
set(gcf,'position',[680 360 860 420]);
set(gca,'FontWeight','bold');

%modify phase data to remove jumps due to going from -180 to 180 by adding
%and subtracting 360 degrees as necessary
m_phase=phase;
for j=2:1:6
    for i=2:1:length(m_phase(:,1))
        if (m_phase(i,j)-m_phase(i-1,j))>200

m_phase(i:1:length(m_phase(:,1)),j)=m_phase(i:1:length(m_phase(:,1)),j)-360;
        end
        if (m_phase(i,j)-m_phase(i-1,j))<-200

m_phase(i:1:length(m_phase(:,1)),j)=m_phase(i:1:length(m_phase(:,1)),j)+360;
        end
    end
end

l1_phase=legend([p1 p2 p3 p4 p5],'1 cm','1.5 cm','2 cm','2.5 cm','3 cm');
```

```
clearvars i j;

%% evaluate phase results

%find frequency ranges with trend
raw_phase=phase;
phase=m_phase;
trend_region_count_phase=0;
trend_length_phase=1;
clearvars trend_index_phase trend_region_lengths_phase
trend_region_starts_phase;
required_sens_phase=0;
for i=1:1:length(phase(:,1))
    %evaluate each frequency to see if there is a trend

trend_down=(phase(i,2)>phase(i,3))&&(phase(i,3)>phase(i,4))&&(phase(i,4)>phas
e(i,5))&&(phase(i,5)>phase(i,6));

trend_up=(phase(i,6)>phase(i,5))&&(phase(i,5)>phase(i,4))&&(phase(i,4)>phase(
i,3))&&(phase(i,3)>phase(i,2));

    %if trend present, keep track of it and surrounding trends
    if trend_down || trend_up
        if exist('trend_index_phase')==0
            trend_index_phase=i;
            trend_region_count_phase=1;
            trend_region_starts_phase=i;
        else
            trend_index_phase=[trend_index_phase i];
            if not(ismember((i-1),trend_index_phase))
                trend_region_count_phase=trend_region_count_phase+1;
                trend_region_starts_phase=[trend_region_starts_phase i];

                if exist('trend_region_lengths_phase')==0
                    trend_region_lengths_phase=trend_length_phase;
                else
                    trend_region_lengths_phase=[trend_region_lengths_phase
trend_length_phase];
                end
                trend_length_phase=1;
            else
                trend_length_phase=trend_length_phase+1;
            end
        end
    end
end
% if a trend was found, continue plotting and analyzing trends
if trend_region_count_phase>0
    if exist('trend_region_lengths_phase')
        trend_region_lengths_phase=[trend_region_lengths_phase
trend_length_phase];
    else
        trend_region_lengths_phase=trend_length_phase;
    end
```

```
    %plot trend regions
    best_freqs=phase(trend_region_starts_phase,1);
    required_sens_region=1;
    for j=1:1:trend_region_count_phase
        if trend_region_lengths_phase(j)>=10 %set to minimum desired trend
bandwidth
            xrange=[phase(trend_region_starts_phase(j),1)
phase(trend_region_starts_phase(j)+trend_region_lengths_phase(j)-1,1)];
            yrange=get(gca,'YLim');
            f1=fill([xrange(1) xrange(1) xrange(2) xrange(2)],[yrange
flip(yrange)],[0, 0.5, 0],'facealpha',0.2,'linestyle','none');

            %determine the change in s21 for each change in radius
            x_index_range=[trend_region_starts_phase(j)
trend_region_starts_phase(j)+trend_region_lengths_phase(j)-1];
            max_gap=zeros(1,4);
            max_index=zeros(1,4);
            gap=zeros(4,length(x_index_range));
            min_gaps=zeros(1,length(x_index_range));
            for
k=trend_region_starts_phase(j):1:(trend_region_starts_phase(j)+trend_region_l
engths_phase(j)-1)
                gap(1,k)=phase(k,2)-phase(k,3);
                gap(2,k)=phase(k,3)-phase(k,4);
                gap(3,k)=phase(k,4)-phase(k,5);
                gap(4,k)=phase(k,5)-phase(k,6);
                min_gaps(k)=min(abs(gap(:,k)));
            end

            %identify the frequency with greatest minimum gap
            [best_min_gap,best_min_gap_index]=max(min_gaps);
            for m=1:1:4
                [max_gap(m),max_index(m)]=max(abs(gap(m,:)));
            end
            [min_max_gap,min_max_gap_index]=min(max_gap);
            best_freqs(j)=phase(best_min_gap_index,1);

            %update required sensitivity
            if (best_min_gap>required_sens_phase)
                required_sens_phase=best_min_gap;
                required_sens_freq_phase=best_freqs(j);
                required_sens_index_phase=best_min_gap_index;
                required_sens_region=j;
            end
        else
            %keep track of trends that don't meet required bandwidth
            if exist('short_trends');
                short_trends=[short_trends j];
            else
                short_trends=j;
            end
        end
    end
```

```
    %remove best trend and any short trends from being plotted as local
    %best
    if exist('short_trends')
        best_freqs([short_trends required_sens_region])=[];
    else
        best_freqs(required_sens_region)=[];
    end

    %plot best trend location for each region
    v1=plot([required_sens_freq_phase required_sens_freq_phase],yrange,'k--
','lineWidth',3);
    for j=1:1:length(best_freqs)
            v2=plot([best_freqs(j)
best_freqs(j)],yrange,'color',[0,0.5,0],'linestyle','-.');
    end

else
    disp('No Phase Trends Found');
end

%display key phase performance results
fprintf('Best Phase Trend Frequency: %f\n',required_sens_freq_phase);
fprintf('Required Phase Sensitivity: %f Degrees\n',required_sens_phase);

l1_phase=legend([p1 p2 p3 p4 p5],'1 cm','1.5 cm','2 cm','2.5 cm','3
cm','location','northeastoutside');
title(l1_phase,'BCS Sphere Radius');
if trend_region_count_phase>0
    ax=axes('Position',get(gca,'Position'),'Visible','Off');
    l2_phase=legend(ax,[f1 v2 v1],'Trend Present','Optimal Freq.
(Local)','Optimal Freq.','location','southeastoutside');%%%%%%%%
    title(l2_phase,'Trend Markers');
    set(gca,'FontWeight','bold');
end

phase=raw_phase;

clearvars p1 p2 p3 p4 p5 best_min_gap best_min_gap_index;
clearvars short_trends trend_index_phase trend_length_phase
trend_region_count_phase trend_region_lengths_phase trend_region_starts_phase
x_index_range;
clearvars best_freqs gap max_index min_max_gap min_max_gap_index
required_sens_region max_gap;
clearvars trend_down trend_up xrange yrange i j k l1_phase m_phase;
clearvars f1 l2_phase v1 v2 ax m min_gaps marker_distance raw_phase;
```